Measurement of Temperature Field of Jet Impingement Over a Concave Surface Using Thermographic Phosphors and CFD Analysis

Yeongmin Jo, Yujin Im, and Eunseop Yeom

Abstract This study analyzed the characteristics of an impinging jet on a concave surface, using thermographic phosphor thermometry (TPT) and numerical method. The experiments were conducted under a jet Reynolds number of 6600, with variations in nozzle diameters (5 and10 mm) and nozzle-to-surface distances (H/d = 2 and 5). The study highlights the accuracy of the RNG k-ε turbulence model in predicting the Nusselt number distribution when compared to alternative models such as SST k-ω and realizable k-ε. The results reveal significant variations in heat transfer characteristics associated with changes in nozzle diameter and H/d (Nozzle to surface distance). A distinctive secondary peak in heat transfer was observed at H/d = 2, attributed to vortex-induced flow detachment and subsequent reattachment. Furthermore, increasing the nozzle diameter was found to enhance jet momentum, turbulence intensity, and overall heat transfer efficiency. This research provides valuable insights into the intricate dynamics of jet impingement on concave surfaces, with potential applications in various engineering fields.

Keywords Impinging Jet · Temperature field · CFD simulation · Concave surface · Thermographic phosphor thermometry (TPT)

1 Introduction

Impinging jets, widely used in industries like turbine blade cooling and electronics manufacturing, require precise temperature distribution measurements on metal surfaces. Traditional methods, such as infrared cameras, temperature-sensitive paints, and thermocouples, face limitations in temperature range, resolution, or necessitate direct contact, complicating flow condition monitoring. This study introduces a non-contact method using thermographic phosphor thermometry (TPT) that exploits phosphorescent material's light-induced emission for temperature measurement,

Y. Jo · Y. Im · E. Yeom (✉)
School of Mechnical Engineering, Pusan National University, Busan, South Korea
e-mail: esyeom@pusan.ac.kr

D. Kim et al. (eds.), *Fluid-Structure-Sound Interactions and Control*, Lecture Notes in Mechanical Engineering, https://doi.org/10.1007/978-981-97-6211-8_36

unaffected by flow conditions. It involves high-speed, high-resolution temperature field visualization through varying jet nozzle diameters and the distance-to-diameter (H/d) ratio on a high-temperature concave surface. The findings, benchmarked against Computational Fluid Dynamics (CFD) simulations, aim to refine simulation accuracy and understand flow characteristics affecting temperature distribution, guiding the selection of the optimal turbulence model for future investigations.

2 Method

2.1 Experimental Method

A polyimide heater (0.3 mm thick) and stainless steel foil (0.1 mm thick) were attached on a concave stainless steel plate (1.5 mm thick). The stainless steel foil was heated uniformly at a constant heat flux using a heater attached underneath it, and Mg4FGeO6:Mn(MFG) powder and HPC binder (ZYP Coatings Inc., Oak Ridge, USA) were mixed at a ratio of 3:1. An airbrush was used to evenly coat the concave surface of the stainless steel foil. UV-LED (Mightech, 365 nm) was used to irradiate The light emitted from the MFG was filmed using a high-speed camera (Phantom VEO710L), and a band-pass filter (Edmund Optics) was installed on the front to allow only light with a wavelength of 655 ± 50 nm to pass through. Finally, a circular jet nozzle (5, 10 mm in diameter) was fixed in the vertical direction, the diameter of the hemispherical plate was 100 mm, the nozzle height was fixed differently depending on H/d (2, 5), and the jet Reynolds number was set to 6600. The images obtained through the camera were converted into temperature fields using a data processing program (MATLAB) [2].

2.2 Numerical Method

The Reynolds-averaged Navier–Stokes (RANS) model is employed for flow analysis, utilizing time-averaged equations. The RANS model was chosen for its suitability in near-wall analysis and computational efficiency [1]. Among the RANS turbulence models, three were utilized for the analysis: RNG k-ε, realizable k-ε, and SST k-ω. The analysis was conducted for two cases: $H/d = 2$ and $H/d = 5$.

In this study, five boundary layers were added to the bottom surface to optimize the calculation domain, employing the element-based finite volume method. The governing equations were integrated over finite control volumes, with a second-order upwind scheme used for discretizing convective terms in the momentum, turbulence, and energy equations. The total number of cells was set at 5,224,031.

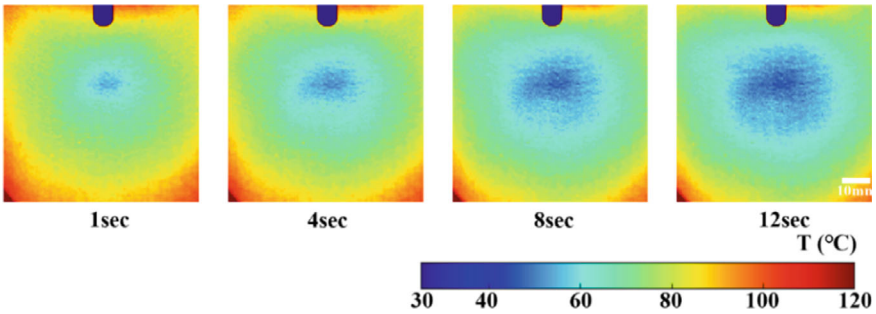

Fig. 1 Transient temperature fields (blue square structure in the upper part represents the nozzle.)

3 Result and Discussion

3.1 Visualization of Transient Temperature Field

Figure 1 illustrates the evolution of the temperature field during this cooling process, as measured using TPT, under constant heat flux conditions caused by the impinging jet. Over time, the expansion of the cooling region can be observed.

Figure 2 presents the comparison of the Nusselt number (Nu) distribution along the X-axis (direction of the concave surface) between Computational Fluid Dynamics (CFD) simulations and actual experiments. In real experiments, the air around the plate gets heated, leading to convection, but this effect is neglected in simulations, resulting in greater cooling at the center. Previous research determined the R^2 (correlation coefficient) value to compare the Nu number distribution in the X/d direction for both simulation and experiment, specifically focusing on a generally hemispherical plate on a concave surface. The experimental data were compared with the data from each simulation model, yielding R^2 values of 0.9816, 0.9840, and 0.9845 for SST, Realizable, and RNG models, respectively. Thus, the RNG k-ε model demonstrates the good agreement with the experimental results.

3.2 Flow and Temperature Distribution

Cooling of hot surfaces by impinging jets primarily occurs through convection, with the most significant heat transfer observed in the stagnation regions where the jet velocity is zero. Flow characteristics were observed based on the simulation previously verified through the Nu number distribution. The transition from axial to radial directions, as depicted in the velocity, pressure, and temperature distributions in Fig. 3, emphasizes the distinctive flow characteristics across the free jet region, stagnation region, and wall jet region. When a jet impinges on the surface, the kinetic energy of the jet flow decreases rapidly at the stagnation point, leading to an increase

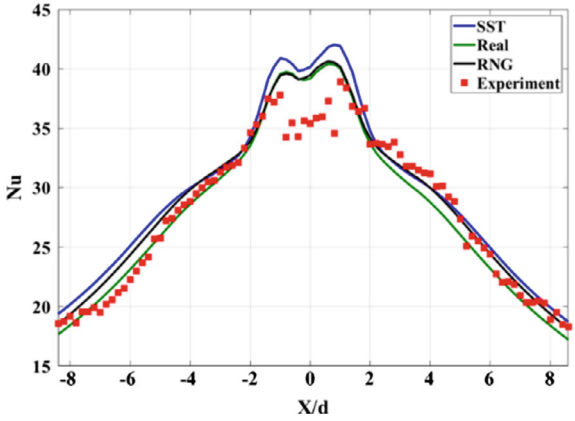

Fig. 2 Comparisons of simulation and experiment data

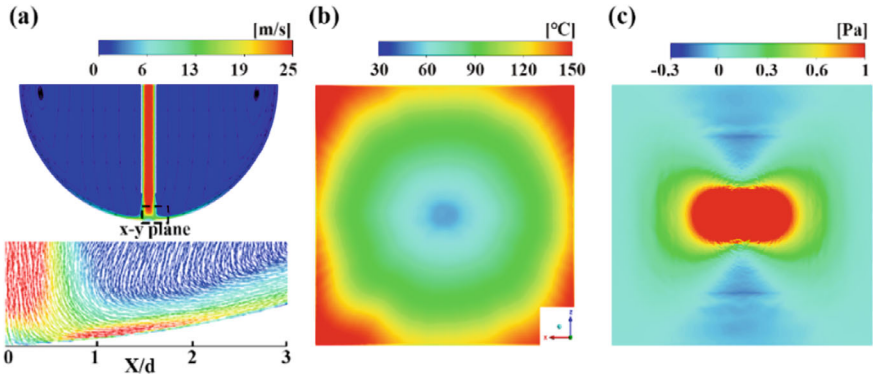

Fig. 3 **a** Velocity stream lines and vectors. **b** Temperature and the **c** pressure fields in x–z plane

in pressure energy that drives the flow radially. This process creates a pronounced pressure gradient near the surface and thins the boundary layer near it. The strong shear layer, resulting from the high radial velocity after the impact, encourages the influx of surrounding air, thereby maximizing heat transfer, especially in the stagnation areas.

3.3 Heat Transfer Characteristics

The experiment was conducted using different nozzle diameters (5 and 10 mm) and various nozzle-to-surface distances (H/d = 2 and 5). Figure 4 results demonstrate variations depending on the nozzle diameter and H/d ratio. For the 5 mm nozzle, at H/d = 2, the Nu number distribution exhibits a relatively flat profile near the peak stagnation point area ($-2.5 < X/d < 2.5$). Conversely, at H/d = 5, it displays a

more pointed shape. When a jet impinges, relatively small H/d (H/d = 2), a vortex structure caused by the entrainment of surrounding air when the jet is ejected from the nozzle extends up to the impinging surface. This vortex structure leads to the formation of a secondary vortex due to a reverse pressure gradient at the point where the boundary layer thickens post the stagnation point, resulting in the boundary layer's separation and reattachment. If a vortex structure causes flow separation along the surface, it leads to a decrease in convective heat/mass transfer coefficients. Conversely, flow reattachment results in an increase in these coefficients, thereby impacting heat transfer along the surface. The compressed flow beneath the vortex induces higher velocity, and the fluid entering the vortex tends to be relatively cold. This leads to an expected increase in mass flow and consequently higher convection rates, leading to a secondary peak structure observed even in the Nusselt number distribution [4]. This Nusselt distribution is noted at low H/d, but at H/d ratios greater than the potential core (H/d = 4), such a structure does not occur, and a gradual decrease in the Nusselt number distribution from the stagnation point is observed. When the nozzle and plate are in close (H/d = 2), a reverse pressure gradient emerges, creating a vortex and an associated region of flow instability. Vortex roll-up occurs within areas of strong adverse pressure gradient, decelerating the fluid layer near the surface while increasing velocity within the shear layer. In Fig. 3a, at the bottom of the shear layer in the velocity distributions, the jet initially reaches maximum velocity upon surface impact, briefly decreases, and then increases again. Furthermore, the overall Nu distribution for the 10 mm nozzle is greater than that for the 5 mm nozzle. As the nozzle diameter increases, the length of the potential core also increases [3]. In simpler terms, for the same H/d, a larger nozzle diameter results in higher average velocity (momentum). Within the potential core, there is a certain level of turbulence intensity, but outside this region, turbulence intensity rapidly escalates as the jet vigorously mixes with the surrounding air. Consequently, the 10 mm nozzle exhibits greater jet momentum and turbulence intensity compared to the 5 mm nozzle, leading to increased heat transfer.

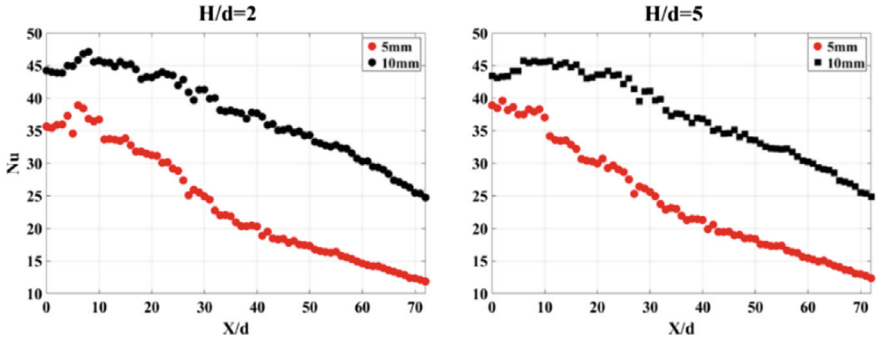

Fig. 4 Comparisons of Nu distribution on variable nozzle diameters depending on H/d values

4 Conclusion

The temperature changes resulting from the impingement of the jet onto the concave surface were effectively translated into temperature fields through TPT, and their distinctive characteristics were verified. This study successfully captured high-resolution temperature fields on concave surfaces in a high-temperature environment using non-contact optical equipment. As a valuable reference for assessing heat flow correlations, this research has yielded meaningful results. It offers insights into the cooling of mechanical components featuring concave shapes where jets impinge, and has the potential to inform the design enhancement process for improved heat transfer efficiency.

References

1. Alimohammadi S, Murray DB, Persoons T (2014) Experimental validation of a computational fluid dynamics methodology for transitional flow heat transfer characteristics of a steady impinging jet. J Heat Transfer 136
2. Kim M, Kim D, Yeom E (2020) Measurement of three-dimensional flow structure and transient heat transfer on curved surface impinged by round jet. Int J Heat Mass Transf 161:120279
3. Lee DH, Song J, Jo MC (2004) The effects of nozzle diameter on impinging jet heat transfer and fluid flow. J Heat Transfer 126:554–557
4. Yadav H, Agrawal A (2018) Effect of vortical structures on velocity and turbulent fields in the near region of an impinging turbulent jet. Phys Fluids 30:035107